Dalton Transactions

An international journal of inorganic chemistry

Accepted Manuscript

Dalton Transactions

An international journal of inorganic chemistry

rsc.li/dalton

Volume 46
Number 10
14 March 2017
Pages 3073-3412

ISSN 0306-0012

COMMUNICATION
Douglas W. Stephan et al
N-Heterocyclic carbene stabilized parent sulfenyl, selenenyl, and tellurenyl cations (XH⁺; X = S, Se, Te)

ROYAL SOCIETY
OF CHEMISTRY

This is an Accepted Manuscript, which has been through the Royal Society of Chemistry peer review process and has been accepted for publication.

Accepted Manuscripts are published online shortly after acceptance, before technical editing, formatting and proof reading. Using this free service, authors can make their results available to the community, in citable form, before we publish the edited article. We will replace this Accepted Manuscript with the edited and formatted Advance Article as soon as it is available.

You can find more information about Accepted Manuscripts in the Information for Authors.

Please note that technical editing may introduce minor changes to the text and/or graphics, which may alter content. The journal's standard Terms & Conditions and the Ethical guidelines still apply. In no event shall the Royal Society of Chemistry be held responsible for any errors or omissions in this Accepted Manuscript or any consequences arising from the use of any information it contains.

ROYAL SOCIETY
OF CHEMISTRY

rsc.li/dalton

ARTICLE

Single and double deprotonation/dearomatization of N,S-donor pyridinophane ligand in ruthenium complexes

Hoan Minh Dinh,[a] Tatiana Gridneva,[a] Ayumu Karimata,[a] Alèria Garcia-Roca,[a] Jiratheep Pruchyathamkorn,[a] Pradnya H. Patil,[a] Andrey Petrov,[a] Abir Sarbajna,[a] Sébastien Lapointe,[a] Eugene Khaskin,[a] Robert R. Fayzullin,[b] and Julia R. Khusnutdinova*[a]

We report a series of ruthenium complexes with a tetradentate N,S-donor ligand, 2,11-dithia[3.3](2,6)pyridinophane (N_2S_2) that undergo single and double deprotonation in the presence of a base leading to the deprotonation of one or both pyridine rings. Both singly and doubly deprotonated complexes were structurally characterized by single-crystal X-ray diffraction. The NMR spectra are indicative of dearomatization of one or both pyridine rings upon deprotonation of the CH_2-S arm, similar to dearomatization of phosphine-containing pincer ligands. The deprotonated (N_2S_2)Ru complexes did not show appreciable catalytic or stoichiometric reactivity in transfer hydrogenation, hydrogenation and dehydrogenation of alcohols, and attempted activation of H_2, CO_2, and other substrates. Such lack of reactivity is likely due to the low stability of the deprotonated species as evident from structural characterization of one of the decomposition products in which shrinkage of the macrocyclic ring occurs via picolyl arm migration.

Introduction

The development and utilization of pyridine-based pincer ligands, which typically coordinate to a transition metal center in a tridentate, meridional fashion, has led to important developments in the understanding of basic coordination chemistry, reactivity, and catalytic properties.[1-3] In particular, the concept of metal-ligand cooperation in bond activation and catalysis, has risen to prominence from studies of metal complexes with PNP pincer ligands, which contain a pyridine substituted with two methylene-bridged phosphine arms. The deprotonation of the acidic CH_2 arm present between the pyridine and phosphine donors leads to pyridine ring dearomatization and gives an amide character to the resulting N-donor. Upon activation of a substrate such as H_2 or other molecules, both the ligand arm and the metal heterolytically cleave the substrate leading to ligand rearomatization (Scheme 1).[1, 4-5]

Further development of different types and structural variations of pincer ligands showed that such reactivity is not limited to phosphine donors and can be also observed for other types of pincer ligands[6] containing sulfide,[7] NHC,[8-9] sulfoxide[10] and amine donors.[11] This is particularly important considering

that the high air sensitivity and the cost of dialkylphosphine ligands may be a limiting factor in industrial catalysis. Replacement of phosphines with other types of "soft" donors such as sulfides, may provide potentially more air-stable and cheaper ligand types with similar reactivity patterns.[12-19]
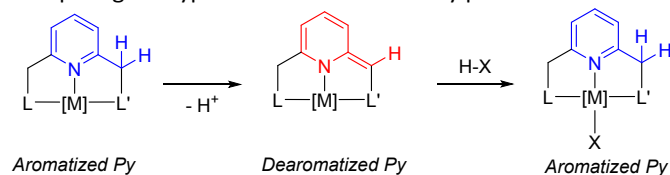
Scheme 1. Pincer ligand deprotonation and reactivity.

At the same time, the development of N,S-donor ligands in catalysis has led to systems being developed that display good catalytic activity in hydrogenation[20-24], transfer hydrogenation[25] and acceptorless dehydrogenation reactions[26-27], sometimes exceeding the performance of phosphine-based donors. However, only a limited number of studies have been reported on the deprotonation reactivity of sulfur-based pincer ligands. For example, the Milstein group has studied the deprotonation of a PNS pincer ligand in Ru complexes, which led to Ru complex dimerization and eventually to an irreversible cleavage of the ligand framework.[7]

Our group has been interested in the study of tetradentate macrocyclic pyridinophane ligands combining two pyridine fragments interconnected with two donor atoms (typically N- or S) via four methylene bridges. This type of ligand may be seen as a superposition of two pincer fragments; however, it shows distinctly different coordination properties and typically binds to a metal in a facial mode either as a κ^3 tridentate or κ^4 tetradentate ligand. The κ^2 bidentate coordination mode is also

[a.] *Okinawa Institute of Science and Technology Graduate University, Coordination Chemistry and Catalysis Unit, 1919-1 Tancha, Onna-son, Okinawa, Japan, 904-0495. Email: juliak@oist.jp.*

[b.] *Arbuzov Institute of Organic and Physical Chemistry, FRC Kazan Scientific Center, Russian Academy of Sciences, 8 Arbuzov Street, Kazan 420088, Russian Federation.*

known (Scheme 2, a).[28-29] Macrocyclic κ^4 coordination of these ligands is known to stabilize unusual oxidation states or other types of reactive species that may not be accessible using other ligand frameworks.[30-32] In particular, we have recently reported double deprotonation of two methylene arms in the N_2S_2 ligand coordinated to Mn, leading to dearomatization of both pyridine arms (Scheme 2, b).[33] Herein, we extend the study of dearomatization in pyridinophane type ligands to the family of ruthenium complexes supported by the N_2S_2 ligand showing both single and double dearomatization modes and an unusual rearrangement of the macrocyclic ligand framework leading to macrocycle ligand shrinkage via pyridine arm migration.
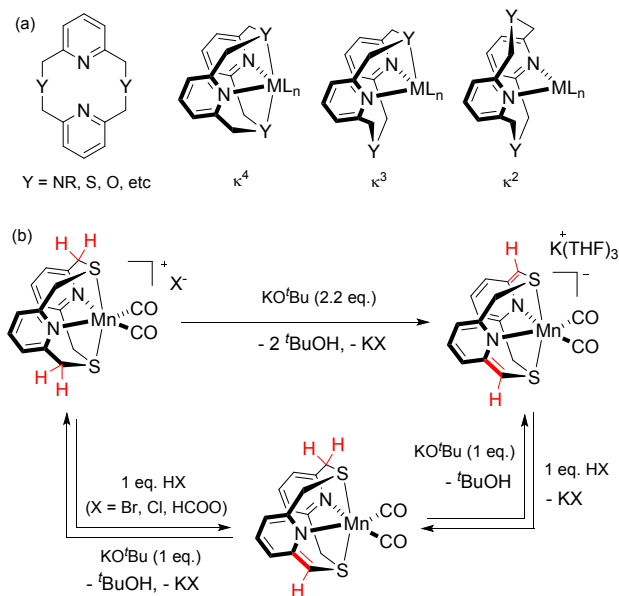
Scheme 2. (a) Pyridinophane ligands and their coordination modes in metal complexes. (b) Deprotonation/dearomatization of $(N_2S_2)Mn(CO)_2^+$ complexes reported in our previous work.

Results and discussion

Synthesis of ruthenium complexes

We examined the reactivity of N_2S_2 ligand with a range of common ruthenium precursors which allowed us to obtain dicationic and monocationic $(N_2S_2)Ru$ complexes. First, $[RuCl_2(p\text{-cymene})]_2$ dimer was pre-treated with silver triflate in acetonitrile solution followed by the addition of N_2S_2 ligand, which yielded the dicationic bis-acetonitrile complex **1** (Scheme 3). Complex **1** was isolated in 64% yield and characterized by NMR, UV-vis, IR spectroscopy and elemental analysis. The ^1H NMR spectrum was consistent with a C_{2v}-symmetrical structure in solution, showing two doublets at 4.76 and 4.74 ppm that correspond to the geminally coupled CH_2 groups of the N_2S_2. The *para*-protons and two equivalent *meta*-protons of pyridine appeared as a triplet at 7.60 and a doublet at 7.38 ppm, respectively. The uncoordinated triflate counteranion appears at −79.25 ppm in the ^{19}F NMR spectrum, ruling out interaction with the ruthenium center. Crystals were obtained by diethyl ether diffusion into an acetonitrile solution

and analysed by single-crystal X-ray diffraction (SC-XRD), showing the expected κ^4-coordination geometry (Figure 1a). Next, the monocationic, chloro-complexes **2** and **3** containing one strongly coordinating ligand, PPh_3 or DMSO, were obtained by the reaction of N_2S_2 with $RuCl_2(PPh_3)_3$ or $RuCl_2(DMSO)_4$, respectively (Scheme 3). Complexes **2** and **3** were isolated in 70-85% yields and characterized by NMR, UV-vis and IR spectroscopy. The κ^4-coordination of N_2S_2 was confirmed by SC-XRD (Figure 1b,c). The $^{31}P\{^1H\}$ NMR spectrum shows the signal of the coordinated phosphine in **2** at 46.28 ppm. The Ru-bound DMSO of **3** appears as a singlet at 3.48 ppm in the ^1H NMR.

In an attempt to obtain ruthenium hydride complex, we then treated a common hydride precursor, $RuHCl(CO)(PPh_3)_3$, with N_2S_2 in toluene/MeOH mixture, however, even after heating at 80 °C for a prolonged time, one of the S-donors of N_2S_2 ligand remained uncoordinated, with N_2S_2 binding in a κ^3-fashion in the resulting complex **4** (Scheme 3). According to SC-XRD, the hydride is present in a *trans*-position to the coordinated S atom, while CO and PPh_3 are located in *trans*-positions to pyridines, and one chloride is present as a counteranion (Figure 1d). The $^{31}P\{^1H\}$ NMR of **4** shows one singlet at 62.90 ppm in CD_2Cl_2 corresponding to the coordinated PPh_3. The IR spectrum shows the CO stretching frequency at 1934 cm^{-1}.

Scheme 3. Synthesis of **1-4**.

Dalton Transactions Accepted Manuscript

ARTICLE
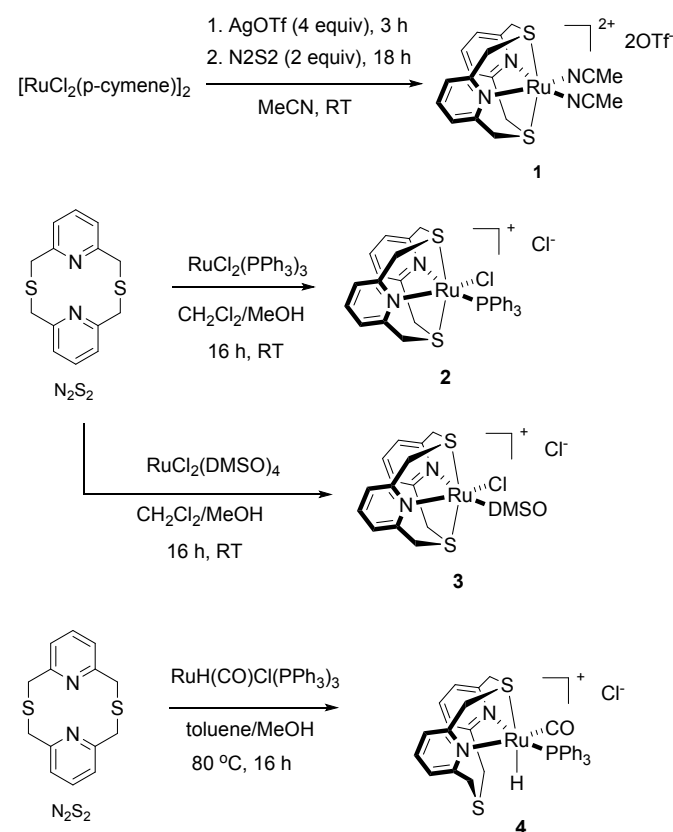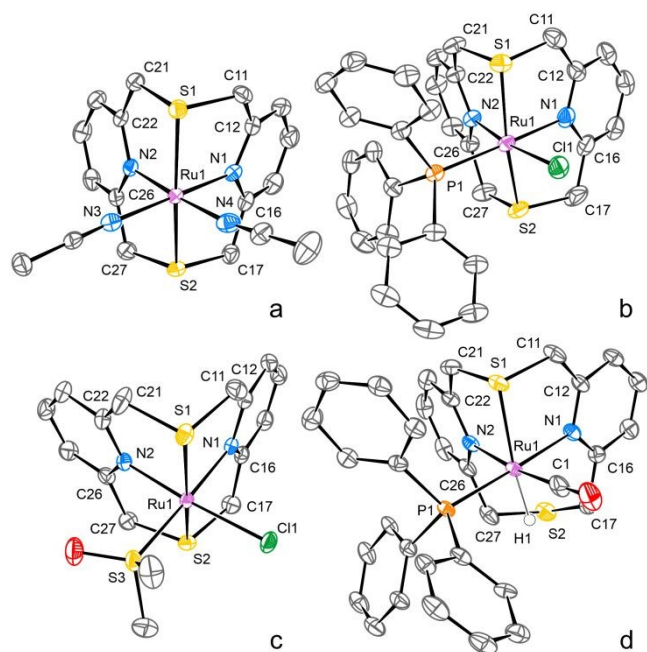
Figure 1. ORTEP of cationic parts of complexes **1** (a), **2** (b), **3** (c) and **4** (d) at 50 % (b, d), 70 % (a) or 80 % (c) probability level according to SC-XRD. Hydrogen atoms, except for [Ru]H1, are omitted for clarity. In the case of **2**, one of two symmetry independent molecules is shown. Selected interatomic distances [Å]: Ru1–S1 2.3226(12), Ru1–S2 2.3144(12), Ru1–N1 2.045(4), Ru1–N2 2.046(4), Ru1–N3 2.054(4), Ru1–N4 2.040(4) for **1**; Ru1–Cl1 2.4315(7), Ru1–S1 2.3228(8), Ru1–S2 2.3186(8), Ru1–P1 2.3070(7), Ru1–N1 2.122(3), Ru1–N2 2.042(2) for **2**; Ru1–Cl1 2.4293(3), Ru1–S1 2.3190(3), Ru1–S2 2.3173(3), Ru1–S3 2.2521(3), Ru1–N1 2.0856(10), Ru1–N2 2.0495(10) for **3**; Ru1–S1 2.3840(15), Ru1–P1 2.2994(14), Ru1–N1 2.219(5), Ru1–N2 2.223(5), Ru1–C1 1.851(7), Ru1–H1 1.60(3) for **4**.

Pyridinophane ligand deprotonation/dearomatization in Ru complexes

Deprotonation of 1. Based on our previous studies of single and double dearomatization of Mn complexes with the N_2S_2 ligand, we expected similar reactivity in (N_2S_2)Ru complexes upon treatment with variable amounts of base.

First, treatment of complex **1** with 2.2 equivalents of KO^{t}Bu in toluene-d_8 gave a poorly soluble doubly deprotonated product **1b** (Scheme 4). Single crystals of **1b** were obtained by cooling a saturated toluene solution at –20 °C and SC-XRD confirmed double deprotonation of the N_2S_2 ligand, with the Ru center retaining two coordinated acetonitrile ligands (Figure 2a). The SC-XRD shows significantly shortened C16=C17 and C21=C22 distances of 1.387(3) and 1.382(3) Å, consistent with double bond character. For comparison, the C11–C12 and C26–C27 distances at the methylene bridges are 1.501(3) Å and 1.502(3) Å respectively, corresponding to a typical C(sp^2)–C(sp^3) bond distance of ca. 1.51 Å. The positions of hydrogen atoms H17 and H21 were determined by difference Fourier maps, and these atoms were refined isotropically. Interestingly, the methine C–S distances at the deprotonated arms are also considerably shorter, 1.730(2) Å and 1.733(2) Å, as compared to the methylene C–S distances of 1.839(2) Å and 1.847(2) Å.

^{1}H NMR and ^{13}C{^{1}H} NMR spectra in toluene-d_8 solution are consistent with double deprotonation: two equivalent CH groups appear as a singlet at 4.18 ppm corresponding to the ^{13}C

signal at 61.4 ppm. The remaining CH$_2$ groups appear as two geminally coupled doublets in ^{1}H NMR spectrum at 3.89 and 3.73 ppm, corresponding to the ^{13}C NMR resonance at 58.23 ppm, as confirmed by the ^{1}H-^{13}C HMQC NMR spectrum. Dearomatization of the pyridine rings resulting from CH$_2$ arm deprotonation is evident from significantly upfield shifted multiplets of the inequivalent pyridine protons at 6.38 (*para*-H) and 6.26 and 5.76 ppm (*meta*-H) (Figure 3).

The doubly deprotonated **1b** was moderately stable in CD$_3$CN, however, it exhibited a diminished intensity of the CH/CH$_2$ signals in ^{1}H NMR due to H/D exchange with CD$_3$CN, showing almost complete deuteration of all CH$_2$ groups after several minutes. We were able to generate **1b** by reacting **1** with 2.2 equivalents of KO^{t}Bu directly in CD$_3$CN in 80% NMR yield based on integration against internal standard. The solution of **1b** slowly decomposes at RT in CD$_3$CN or toluene-d_8. For example, when **1b** was generated by deprotonation of **1** with 2 equiv. of KO^{t}Bu, only about half of the initially formed complex remained in solution after 10 min at RT, forming an insoluble precipitate. Attempts to improve the stability by using a ruthenium complex with two pivaloylnitrile ligands instead of MeCN were unsuccessful and doubly dearomatized species still showed slow decomposition at RT in toluene-d_8.
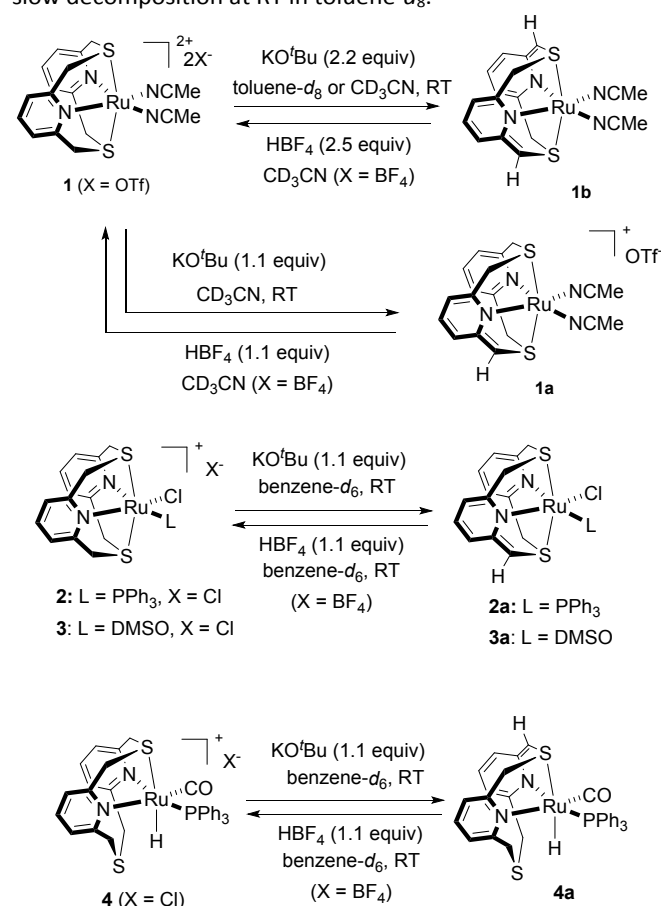
Scheme 4. Deprotonation of **1-4** and reversible protonation of products by HBF$_4$.
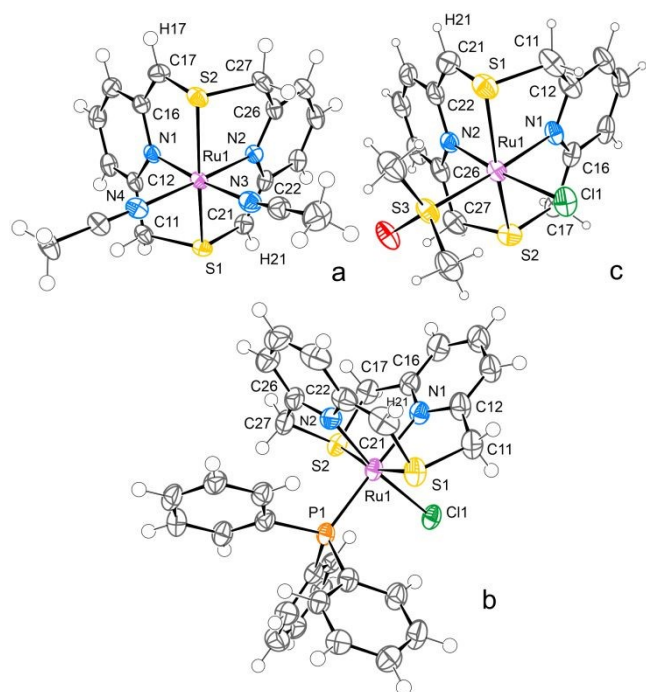
Figure 2. ORTEP of complexes **1b** (a), **2a** (b) and **3a** (c) at 70 % (a, b) or 30 % (c) probability level according to SC-XRD. In the case of **1b**, one of two symmetry independent molecules is shown. The minor disorder component for **3a** and solvent molecules are omitted for clarity. Selected interatomic distances [Å]: Ru1–S1 2.3441(5), Ru1–S2 2.3280(5), Ru1–N1 2.0416(18), Ru1–N2 2.0425(17), Ru1–N3 2.0473(19), Ru1–N4 2.0461(19) for **1b**; Ru1–Cl1 2.4548(6), Ru1–S1 2.3229(7), Ru1–S2 2.3196(7), Ru1–P1 2.2950(7), Ru1–N1 2.099(2), Ru1–N2 2.052(2) for **2a**; Ru1–Cl1 2.442(2), Ru1–S1 2.329(3), Ru1–S2 2.316(2), Ru1–S3 2.235(5), Ru1–N1 2.104(7), Ru1–N2 2.061(7) for **3a**.
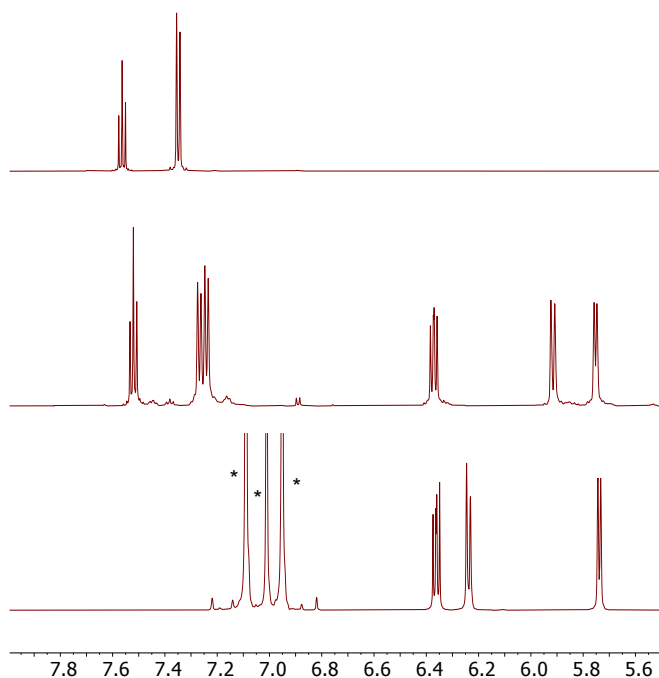
Figure 3. Pyridine peaks in ^{1}H NMR spectra of **1** (top; in CD$_3$CN), **1a** (middle; in CD$_3$CN) and **1b** (bottom; in toluene-d_8). Peaks of residual toluene are marked with an asterisk.

Next, we attempted generation of a monodeprotonated species from **1** in toluene-d_8, but the reaction of **1** with 1.1 equiv. of KO^{t}Bu in toluene-d_8 still resulted in the formation of neutral **1b** as the only species present in solution, along with an insoluble product that may have been the expected but poorly soluble monocationic product. In contrast, the analogous reaction in CD$_3$CN resulted in the generation of the expected monodeprotonated complex **1a** (98% NMR yield), which was characterized by NMR in solution, but could not be isolated in an analytically pure form, as the complex decomposes in solution over the course of several hours.

The ^{1}H NMR resonances in dearomatized pyridine appear as a set of three upfield shifted multiplets at 6.38, 5.94 and 5.77 ppm, whereas the aromatic pyridine protons appear in the 7.25-7.54ppm range, with peak assignment confirmed by a COSY experiment. In CD$_3$CN solution, the methylene and methine groups undergo partial H/D exchange: after initial reaction with a base, their integration is about 70% of expected integration for methine and methylene protons.

Both complexes **1b** and **1a** can be protonated back to fully protonated [(N$_2$S$_2$)Ru(MeCN)$_2$]$^{2+}$ by reacting with HBF$_4$ showing that their deprotonation is reversible.

Unfortunately, single crystals of **1a** could not be obtained, and as an alternative route to monodeprotonated species, we tested the reactivity of monocationic complexes **2-4** with base. We anticipated that single deprotonation of these complexes would lead to the formation of neutral species and will thus improve their solubility and stability in nonpolar solvents.

Deprotonation of monocationic complexes 2-4.

When monocationic phosphine complex **2** was reacted with 1.1 equivalent of KO^{t}Bu in benzene-d_6, a new singly deprotonated complex **2a** was obtained in 88% yield, crystallized by vapor diffusion of pentane into a benzene solution. The X-ray structure confirms that **2a** is a neutral complex with Cl and PPh$_3$ coordinated to Ru (Figure 2b). The N$_2$S$_2$ ligand is singly deprotonated with one CH and three CH$_2$ arms as confirmed by X-ray and NMR. The SC-XRD structure reveals one shortened C21=C22 bond (1.368(4) Å), whereas the other C11–C12, C16–C17 and C26–C27 bond distances are 1.501(4) Å, 1.504(4) Å and 1.500(4) Å, respectively. Similarly, the methine C–S bond is also shortened, 1.744(3) Å, as compared to the methylene C–S bond distances (1.852(3), 1.829(3) and 1.828(3) Å).

The ^{1}H and ^{13}C{^{1}H} NMR spectra in benzene-d_6 were also consistent with singly deprotonated species showing a singlet for the methine group at 3.86 ppm that corresponded to the ^{13}C signal at 65.0 ppm as confirmed by DEPT and HMQC spectroscopy, while the proton resonances of CH$_2$ groups appear as a set of six doublets in ^{1}H NMR at 2.76-4.81 ppm. The protons of the dearomatized pyridine ring are upfield shifted (5.06, 5.92 and 6.04 ppm) as compared to the protons of the aromatic pyridine ring (6.06, 6.29 and 6.33 ppm).

The monocationic DMSO-coordinated complex **3** reacted in a similar way with 1.1 equivalents of KO^{t}Bu in benzene-d_6 solution to give monodeprotonated complex **3a** in 57% yield, which was also characterized by NMR and SC-XRD. Dearomatized pyridine signals appear upfield shifted (5.46, 5.89, and 6.21 ppm) as compared to the aromatic pyridine multiplets (6.03-6.32 ppm),

although the change in the chemical shifts is less pronounced compared to **2a**. Similar to **2a**, six doublets of methylene groups and one methine proton singlet (3.86 ppm) are also present in ^1H NMR. SC-XRD reveals an S-coordinated DMSO neutral complex, which structure shows one pair of shortened C21=C22 (1.406(17) Å) and S1–C21 (1.681(15) Å) bonds (Figure 2c). Comparison of selected interatomic distances of the studied complexes is given in Table 1.

Both complexes **2a** and **3a** showed noticeable decomposition when an excess of base (2 equiv. and more) was present, forming a mixture of unidentified products.

The reaction of κ^3 coordinated hydride complex **4** with 1.1 equiv. of KO^{t}Bu in benzene-d_6 also gave a singly deprotonated complex **4a**, which undergoes selective deprotonation at the CH$_2$ arm while the Ru–H remains intact. The same product was obtained when up to 3 equiv of KO^{t}Bu was added (96-99% *in situ* NMR yield of **4a**, with a slightly diminished yield when 4 equiv of base was used (see ESI)). Accordingly, ^1H NMR shows a Ru–H peak at −6.55 ppm as a doublet due to phosphorus splitting (J_{HP} = 28.8 Hz), a singlet CH peak at 3.81 ppm and a set of six doublets from geminally coupled CH$_2$ groups. Interestingly, even in the presence of excess base (up to 3

equiv.), **4a** remained as the main component (96-99% yield). Unfortunately, we were unable to obtain a single crystal of **4a**, however, we hypothesized that deprotonation occurs at the CH$_2$S arm coordinated to Ru center, rather than on a dangling S-containing fragment. This is consistent with the results of the comparison of the relative Gibbs free energies for the DFT-optimized structures of several possible isomers of **4a** (Figure 4), showing that the most stable isomer corresponds to the structure **4a-A** with the deprotonated CH$_2$S coordinated to the Ru center, while deprotonation of the dangling S-arm is highly unfavourable.

All singly deprotonated complexes **2a**-**3a** react with HBF$_4$ to fully recover the [(N$_2$S$_2$)RuCl(L)]$^+$ core (L = PPh$_3$ or DMSO) confirming that similar to **1a**, their deprotonation is reversible. At the same time, protonation of the ligand's methine group does not occur when **2a**-**4a** are treated with 1.1 equiv of methanol and the complexes remain unreacted. Interestingly, protonation of **4a** obtained by first deprotonation with 1.1 equiv of base and then 1.1 equiv of HBF$_4$, selectively recovers the hydride complex [(κ^3-N$_2$S$_2$)RuH(CO)(PPh$_3$)]$^+$, with the hydride ligand remaining unaffected by strong acid.

Table 1. Selected bond distance (Å) for complexes **1-4** and their deprotonated species according to SC-XRD data[a]

Complex	S1–C11	S1–C21	S2–C17	S2–C27	C11–C12	C16–C17	C21–C22	C26–C27
1	1.825(5)	1.822(5)	1.810(5)	1.823(5)	1.494(6)	1.496(6)	1.499(6)	1.494(6)
1b[b]	1.847(2)	1.733(2)	1.730(2)	1.839(2)	1.501(3)	1.387(3)	1.382(3)	1.502(3)
2[b]	1.821(4)	1.817(3)	1.818(4)	1.812(3)	1.501(5)	1.497(5)	1.497(4)	1.503(4)
2a	1.852(3)	1.744(3)	1.829(3)	1.828(3)	1.501(4)	1.504(4)	1.368(4)	1.500(4)
3	1.8158(13)	1.8198(13)	1.8140(12)	1.8181(12)	1.4964(17)	1.4990(16)	1.5017(17)	1.4998(16)
3a	1.832(11)	1.681(15)	1.837(11)	1.795(12)	1.456(17)	1.459(16)	1.406(17)	1.471(16)
4	1.791(7)	1.791(7)	1.834(8)	1.829(7)	1.504(9)	1.497(9)	1.508(9)	1.498(10)

[a] Atom numbering corresponds to that of Figures 1 and 2. [b] There are two complexes in the asymmetric cell, data are tabulated for the first complex.

Relative Gibbs free energies (kcal mol^{-1}):

4a-A	**4a-B**	**4a-B**	**4a-D**
0	1.78	20.8	20.5
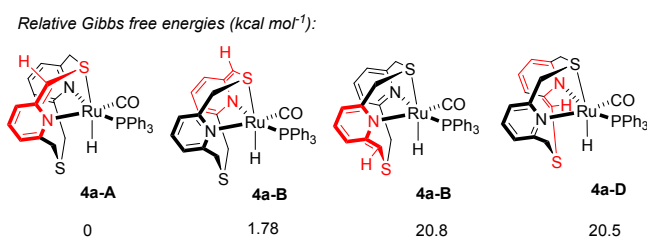
Figure 4. Relative Gibbs free energies (kcal mol^{-1}) for DFT-optimized isomers of **4a** (M06/SDD(Ru), 6-311+g(d,p); SMD solvation in benzene).

Reactivity of deprotonated complexes.

With the initial aim to use the deprotonated N$_2$S$_2$ metal complexes in new types of metal-ligand cooperation, we set out to investigate the reactivity of doubly as well as singly deprotonated complexes with a range of small molecules typically used to study MLC activation in phosphine complexes. To our disappointment, under a range of conditions, both **1b** and **2a** were unreactive towards H$_2$ and terminal acetylenes. Reactions with CO$_2$ and CS$_2$ led to the formation of insoluble products, which produced a mixture of products or decomposition to black precipitate when dissolved in polar

solvents. We then investigated if these complexes may be used as catalysts for hydrogenation or transfer hydrogenation. Unfortunately, no catalytic reactivity was observed in hydrogenation or transfer hydrogenation of acetophenone using catalytic amounts of **1-4** in the presence of base. The complexes **1b** were also inactive in nitrile hydration of acetonitrile, dehydrogenation of benzyl alcohol, and hydrogenation of benzonitrile or benzyl benzoate.

One of the reasons for the lack of catalytic activity could be due to the presence of strongly coordinating ligands. For example, in complex **1** and its deprotonated forms, MeCN remains coordinated to Ru after deprotonation, while in complexes **2** and **3**, coordinated chloride persists even after treatment with a base. While displacement of these ligands (especially MeCN) to enable substrate activation could be possible under forcing conditions, the intrinsic instability of the deprotonated sulfide-containing ligand under strongly basic conditions is likely to lead to irreversible decomposition prior to substate activation or catalytic turnover. In this regard, irreversible defragmentation of the sulfide-containing PNS ligand framework in Ru complexes was earlier reported by the Milstein group.[7] Indeed, while studying deprotonation of **2** with excess (3.6 equiv.) of KO^{t}Bu or NaH in THF, we found that after prolonged time at RT, a mixture

of products formed, from which a rearrangement product **5** could be isolated and crystallized.
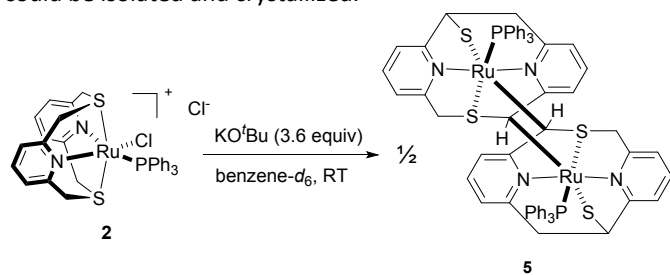
Scheme 5. Formation of **5**.
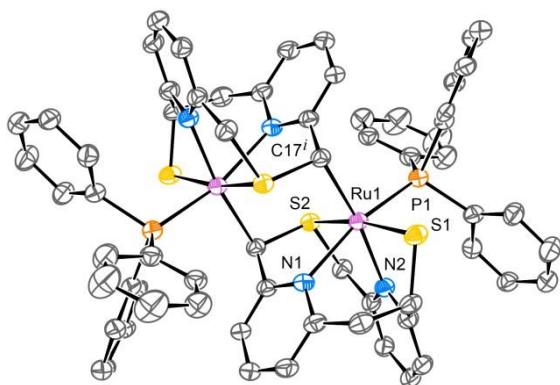
Figure 5. ORTEP for **5** at 30 % probability level according to SC-XRD. Hydrogen atoms and minor disorder components are omitted for clarity. Selected interatomic distances [Å]: Ru1–S1 2.3758(9), Ru1–S2 2.2996(8), Ru1–P1 2.2713(10), Ru1–N1 2.297(3), Ru1–N2 2.080(3), Ru1–C17^i 2.194(3) (symmetry code i: 5/3–x, 4/3–y, 4/3–z).

Single crystals of **5** were obtained by diffusing hexane vapor into a toluene solution of the deprotonation reaction mixture. X-ray diffraction analysis revealed that complex **5** is a centrosymmetric binuclear species, in which the N_2S_2 ligand undergoes macrocycle ring "shrinkage" via the 1,2-migration of a picolyl CH_2 carbon from sulfur to the CH arm (Figure 5). In effect, the sulfur atom becomes an anionic donor for the Ru center while the pyridine ring is re-aromatized. Each of the Ru atoms is also coordinated to the remaining deprotonated CH arm of the counterpart ligand with Ru–C bond distances of 2.194(3) Å, inducing re-aromatization of the second pyridine ring and resembling dimerization in ruthenium complexes with PNS pincer ligand upon deprotonation reported by the Milstein group. The structure of **5** was also confirmed by NMR spectroscopy. The ^1H NMR spectrum of **5** in THF-d_8 exhibits four sets of doublets for the two methylene groups, showing correlation to the carbon CH_2 peaks at 59.93 and 58.87 ppm, based on DEPT and HMQC NMR analyses. The two CH groups appear as singlets at 3.47 and 3.58 ppm, corresponding to the ^{13}C peaks at 64.35 and 63.48 ppm.

The picolyl arm migration to deprotonated CH–S arm resembles Stevens rearrangement in sulfonium salts in the presence of a strong base via generation of sulfonium ylides.[34-37] In Stevens rearrangement, 1,2-migration of the alkyl group occurs from the cationic sulfur atom to the anionic site, typically formed by deprotonation of the -CH_2-$S(Alk)_2^+$ group of sulfonium salts by a strong base. Although no sulfonium group is present in N_2S_2, such reactivity at sulfur could be induced due to coordination to a cationic ruthenium center, while experimentally observed deprotonation of one CH_2-S generates an anionic center similar to that in sulfonium ylides, to which an adjacent picolyl arm migrates; the unusual extrusion of sulfur into exocyclic position could be driven by the product stabilization via coordination of an anionic sulfide to ruthenium atom. The formation of **5** suggests that intrinsic reactivity of the sulfide-containing pincer framework could be one of the reasons for lack of catalytic reactivity and irreversible ligand decomposition in the presence of a base. Interestingly, picolyl arm migration in a pincer-like framework has also been observed in other types of pincer-type ligands. For example, Khaskin et al. reported picolyl arm migration in a functionalized PNP pincer ligand leading to the chelate ring expansion and eventually responsible for the loss of catalytic activity.[38] Thus, the pincer ligand framework that has generally been believed to be highly stable due to strong chelation may be a subject of significant rearrangements under basic conditions leading to changes in metal's coordination environment and therefore changes in the catalytic or stoichiometric reactivity.

DFT calculations.

To further analyze changes in the ligand framework that occur during single and double deprotonation and dearomatization, DFT calculations were carried out to compare **1b** and the cationic parts of complexes **1** and **1a**. The geometries were optimized using M06 functional and SDD (for Ru)/6-311+g(d,p) (for other elements) basis set, which were previously used to analyse structures of dearomatized Ru pincer complexes and gave the best agreement with SC-XRD stuctures (see ESI). SMD model was used to account for solvation in toluene. First, to explain the observed selectivity of deprotonation of two CH_2 groups at the opposite sites of the N_2S_2 ligand framework during double deprotonation established by SC-XRD and NMR, we compared three possible isomers of complex **1b**: the experimentally observed **1b**, as well as alternative isomers **1b**-**A** and **1b**-**B** where deprotonation occurs at the CH_2 sites attached to the same pyridine rings or to the same S-atom, respectively. Both alternative solution-optimized isomers were found to be significantly less stable than **1b** (Figure 6), consistent with the experimentally observed **1b** as the only detected isomer, which is not unexpected considering that such double deprotonation around the same pyridine or sulfide fragment is a challenging transformation even for phosphine derivatives.[39-40]

Relative Gibbs free energies (kcal mol^{-1}):
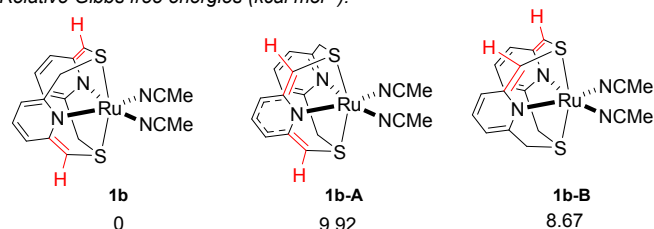
Figure 6. Relative Gibbs free energies (kcal mol⁻¹) for DFT-optimized isomers of **1b** (M06/SDD(Ru), 6-311+g(d,p); SMD solvation in toluene).

The Wiberg bond indices (WBI) and partial atomic charges (Truhlar's Charge Model 5, CM5) were calculated for DFT solution-optimized structures for fully aromatized complex **1**, singly deprotonated **1a**, and doubly deprotonated **1b** (Table 2). While the C-C bond between the methylene groups and pyridine *ortho*-carbon in complex **1** and in non-dearomatylzed pyridine ring in **1b** has a single bond character (WBI 1.0), deprotonation of the CH₂ group to form **1a** or **1b** is accompanied by an increase of the bond index at the deprotonation site (WBI 1.4), suggesting that it acquires double bond character. Upon deprotonation, the "broken" aromatic system of the pyridine ring is characterized by alternating bonds acquiring single and double bond character, consistent with deprotonation-induced dearomatization of the pyridine ring. In a singly dearomatized **1a**, the alternating single/double bond system is only observed at the pyridine ring attached to methine, while no significant changes occur at the opposite pyridine ring attached to two methylene arms that is characterized by bond indices similar to that in **1**.

Table 2. Selected Wiberg bond indices and Partial Atomic Charges (Turhlar's CM5 Model) for optimized structures of 1 (cationic part), 1a (cationic part) and 1b.

Bond	Wiberg bond index			Atom	CM5 charge		
	1	1a	1b		1	1a	1b
N1-C2	1.29	1.16	1.16	Ru1	0.83	0.83	0.83
N1-C6	1.30	1.25	1.27	N1	-0.38	-0.42	-0.41
N2-C9	1.29	1.31	1.16	N2	-0.38	-0.37	-0.41
N2-C13	1.30	1.28	1.27	S1	0.05	0.00	-0.04
S1-C1	0.98	1.09	1.08	S2	0.05	0.01	-0.04
S1-C14	0.98	0.89	0.90	C1	-0.11	-0.20	-0.21
S2-C7	0.98	0.97	0.90	C2	0.13	0.10	0.10
S2-C8	0.98	0.98	1.08	C3	-0.06	-0.10	-0.11
C1-C2	1.03	1.44	1.43	C4	-0.03	-0.07	-0.09
C2-C3	1.42	1.19	1.19	C5	-0.06	-0.13	-0.14
C3-C4	1.41	1.61	1.59	C6	0.13	0.10	0.11
C4-C5	1.42	1.26	1.28	C7	-0.11	-0.12	-0.14
C5-C6	1.41	1.49	1.46	C8	-0.11	-0.12	-0.21
C6-C7	1.03	1.03	1.03	C9	0.13	0.13	0.10
C8-C9	1.03	1.02	1.43	C10	-0.06	-0.08	-0.11
C9-C10	1.42	1.40	1.19	C11	-0.03	-0.05	-0.09
C10-C11	1.41	1.43	1.59	C12	-0.06	-0.07	-0.14
C11-C12	1.42	1.41	1.28	C13	0.13	0.13	0.11
C12-C13	1.41	1.41	1.46	C14	-0.11	-0.14	-0.14
C13-C14	1.03	1.04	1.03				
Ru1-N1	0.44	0.48	0.47				
Ru1-N2	0.44	0.44	0.47				
Ru1-S1	0.49	0.50	0.47				
Ru1-S2	0.49	0.45	0.47				

1   **1a**   **1b**
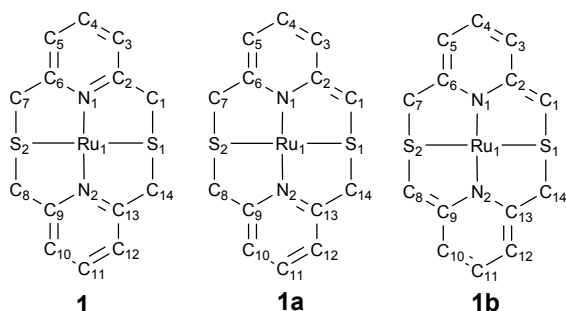
Analysis of CM5 charges in **1b** shows that negative charge accumulation is observed mainly at the methine carbons and the N-atoms of dearomatized pyridine ring, and to a much lesser extent at the meta-carbons. In singly deprotonated **1a**, the negative charge build-up occurs in dearomatized pyridine ring only, in a similar manner to **1b**, while the charge distribution in the aromatic pyridine ring is similar to that in non-deprotonated **1**.

Overall, the analysis of WBI and partial atomic charges in the N,S-donor N₂S₂ macrocyclic ligand suggests that upon deprotonation of one or two methylene arms, the adjacent pyridine ring undergoes partial dearomatization, and thus the N-atom of the dearomatized pyridine acquires amide donor character, similar to the changes that occur in PNP-type pincer ligands.[40]

Conclusions

We reported a series of ruthenium(II) complexes supported by an N,S-donor pyridinophane ligand. Similar to the analogous manganese(I) complexes, ruthenium(II) dicationic, as well as monocationic and neutral complexes, undergo single or double deprotonation of the CH₂S arms leading to dearomatization of the pyridine ring. Compared to many examples of deprotonated ruthenium complexes with N,P-donor pincer ligands reported in the literature, the deprotonated (N₂S₂)Ru complexes show diminished stability, which is the main factor that precludes their use in selective bond activation. One of the decomposition products was identified as the result of rearrangement of the macrocyclic ring leading to macrocycle size shrinkage and extrusion of sulfur into the exocyclic position. The computational analysis confirms that deprotonation of one or

both methylenes in macrocyclic N_2S_2 ligand causes dearomatization of the pyridine ring, resembling the pyridine dearomatization observed upon deprotonation of acyclic, phosphine-based PNP pincer ligands.

Experimental

General specification

All reactions were carried out using Schlenk or glovebox techniques under dry nitrogen/argon atmosphere unless stated otherwise. Anhydrous solvents were dispensed from an MBRAUN solvent purification system and degassed before use. Anhydrous deuterated solvents were purchased from Eurisotop and stored over 4 Å molecular sieves. Unless noted otherwise, all chemicals were purchased from major commercial suppliers (TCI, Sigma-Aldrich, and Nacalai Tesque) and used without purification. NMR spectra were measured on JEOL ECZ400S 400MHz, JEOL ECZ600R 600 MHz, Bruker Avance II 400 MHz and Bruker Avance III 500 MHz. The following abbreviations are used for describing NMR spectra: s (singlet), d (doublet), t (triplet), vt (virtue triplet), q (quartet), dd (doublet of doublets), m (multiplet), quat (quaternary carbon). Residual solvent peaks or internal standard was used as a reference for chemical shifts in ^{1}H NMR spectra. Electrospray Ionization Mass Spectrometry (ESI-MS) measurements were performed on a Thermo Scientific ETD apparatus using MeOH or MeCN as a solvent for injection. Elemental analyses were performed using an Exeter Analytical CE440 instrument. Solid-state FT-IR spectra were measured using Agilent Cary 630 with ATR module in an argon-filled glovebox. The following abbreviations are used for describing FT-IR spectra: s (strong), m (medium), w (weak), br (broad). UV-vis spectra were recorded on an Agilent Cary 60 spectrophotometer. The X-ray diffraction data for the single crystals **1-5**, **1b**, **2a** and **3a** were collected on a Rigaku XtaLab PRO instrument. N_2S_2 ligand was synthesized according to the literature procedure. [41]

Synthesis of complex 1, [Ru(N₂S₂)(MeCN)₂](OTf)₂.

In a glove box, 155 mg (0.253 mmol) of dichloro(p-cymene)ruthenium(II) dimer was dissolved in 12 mL of acetonitrile. To the red solution, 260 mg (1.012 mmol, 4 equiv.) of AgOTf was added and the mixture was stirred in the dark for 3 hours. The AgCl precipitation was then filtered off, and 136 mg (0.495 mmol, 2 equiv.) of N_2S_2 ligand was added. The resulting solution was stirred for 18 hours. The mixture was filtered through celite to remove the remaining AgCl precipitation to give a yellowish-orange solution. The obtained solution was subsequently evaporated to give a yellowish-orange solid, which was washed thrice with a copious amount of ether and pentane and then dried to produce **1**. Yellowish orange crystals were grown by vapor diffusion of diethyl ether to the saturated acetonitrile solution of **1**. Yield: 244 mg (0.323 mmol - 64%). ^{1}H NMR (600 MHz, 23 °C, CD₃CN): δ 7.60 (t, $^3J_{HH}$ = 7.9 Hz, p-H_{Py}, 2H), 7.38 (d, $^3J_{HH}$ = 7.9 Hz, m-H_{Py}, 4H), 4.76, 4.74 (ABq, J_{AB} = 18 Hz, Py–CH_2–S, 8H), 2.35 (s, NC–CH_3, 6H). ^{13}C{^{1}H} NMR (151 MHz, 23 °C, CD₃CN): δ 162.29 (quat. C_{Py}), 137.35 (p-C_{Py}), 130.28 (SO₃–CF₃), 123.05 (m-C_{Py}), 48.43 (Py–CH₂–S), 4.74

(NC–CH₃). ^{19}F NMR (376 MHz, 23 °C, CD₃CN): δ −79.25 (SO₃–CF₃). EA Found (Calculated) C₂₀H₂₀N₄O₆F₆RuS₄: C 31.78 (31.79), H 2.67 (2.67), N 7.41 (8.00). ESI-HRMS (m/z): calculated for [C₁₈H₂₀N₄RuS₂]$^{2+}$: 230.0082; Found: 230.0086. FT-IR (ATR, solid): 2980 (br), 2915 (br), 1602 (m), 1596 (br), 1463 (m), 1406 (m), 1257 (s), 1222 (m), 1148 (s), 1027 (s), 915 (m), 856 (m), 775 (m), 750 (m). UV-Vis (CH₃CN), λ, nm (ε, M⁻¹ cm⁻¹): 344 (8670), 250 (9723), 213 (21954).

Synthesis of complex 2, [Ru(N₂S₂)(PPh₃)Cl]Cl

In a glove box, 174.2 mg (0.182 mmol) of dichlorotris(triphenylphosphine)ruthenium(II) and 51.6 mg (0.188 mmol, 1.0 equiv.) of N_2S_2 ligand were dissolved in 5.0 mL of dichloromethane in a 20 mL vial to give a dark red solution. The reaction mixture was stirred at room temperature for 16 hours, during which time the solution color gradually changed to yellow. The obtained solution was subsequently evaporated at reduced pressure to give a yellow solid, which was washed with ether (3 × 5 mL) and a 1:1 dichloromethane and ether mixture (3 × 5 mL) and then dried to produce **2.** Yellow needle crystals were grown by vapor diffusion of diethyl ether into the dichloromethane solution of the complex. Yield: 109 mg (0.154 mmol - 85%). ^{1}H NMR (600 MHz, 23 °C, CD₂Cl₂): δ 7.54-7.12 (m, H_{PPh3} and H_{Py}, 21H), 5.29 (d, $^2J_{HH}$ = 17.1 Hz, Py–CH_2–S, 2H), 5.10 (d, $^2J_{HH}$ = 17.9 Hz, Py–CH_2–S, 2H), 4.82 (d, $^2J_{HH}$ = 17.0 Hz, Py–CH_2–S, 2H), 3.37 (d, $^2J_{HH}$ = 17.5 Hz, Py–CH_2–S, 2H). ^{13}C{^{1}H} NMR (151 MHz, 23 °C, CD₂Cl₂): δ 161.22 (quat. C_{Py}), 159.02 (quat. C_{Py}) 136.59 (p-C_{Py}), 134.29 (d, $^1J_{PC}$ = 47.0 Hz, quat. CP), 133.84 (m-C_{Py}), 133.61 (d, $^2J_{PC}$ = 10.3 Hz, o-CP), 130.59 (m-C_{Py}), 128.74 (d, $^3J_{PC}$ = 9.4 Hz, m-CP), 122.18 (d, $^2J_{PC}$ = 25.3 Hz, p-CP), 50.34 (Py–CH₂–S), 48.98 (Py–CH₂–S). ^{31}P{^{1}H} NMR (162 MHz, 23 °C, CD₂Cl₂): δ 46.28 (PPh₃). EA Found (Calculated) C₆₅H₆₀Cl₆N₄P₂Ru₂S₄ (2Ru(N₂S₂)(PPh₃)Cl)Cl·1CH₂Cl₂): C 52.07 (51.97), H 3.90 (4.03), N 3.85 (3.73); the presence of CH₂Cl₂ per two Ru complexes in isolated crystals was confirmed by SC-XRD. ESI-HRMS (m/z): Found (Calcd): C₃₂H₂₉N₂ClPRuS₂⁺: 673.0231 (673.0236). FT-IR (ATR, solid) : 3057 (m), 2924 (m), 2858 (m), 1595 (m), 1590 (m), 1457 (m), 1431 (m), 1185 (m), 1155 (m), 1091 (s), 910 (m), 856 (m), 776 (m), 747 (s), 694 (s). UV-Vis (CH₂Cl₂), λ, nm (ε, M⁻¹ cm⁻¹): 379 (5843).

Synthesis of complex 3, [Ru(N₂S₂)(DMSO)Cl]Cl.

In a glove box, 87.7 mg (0.182 mmol) of dichlorotetrakis(dimethylsulfoxide)ruthenium(II) and 50.0 mg (0.182 mmol, 1.0 equiv.) of N_2S_2 ligand were dissolved in a 5.0 mL mixture of 2:1 dichloromethane and methanol in a 20 mL vial to give a yellow solution. The reaction mixture was stirred at room temperature for 16 hours. Yellow needle crystals were grown by vapor diffusion of diethyl ether into the obtained solution of complex to produce **3**. Yield: 67.0 mg (0.128 mmol - 70%). ^{1}H NMR (600 MHz, 23 °C, CDCl₃): δ 7.53 (d, $^3J_{HH}$ = 7.0 Hz, m-H_{Py}, 2H), 7.50 (t, $^3J_{HH}$ = 7.4 Hz, p-H_{Py}, 1H), 7.43 (d, $^3J_{HH}$ = 7.5 Hz, m-H_{Py}, 1H), 7.35 (t, $^3J_{HH}$ = 7.8 Hz, p-H_{Py}, 1H), 5.67 (d, $^2J_{HH}$ = 17.8 Hz, Py–CH_2–S, 2H), 5.64 (d, $^2J_{HH}$ = 17.4, Py–CH_2–S, 2H), 4.74 (d, $^2J_{HH}$ = 17.6 Hz, Py–CH_2–S, 2H), 4.69 (d, $^2J_{HH}$ = 17.8 Hz, 2H), 3.48 (s, (CH_3)₂SO, 6H). ^{13}C{^{1}H} NMR (151 MHz, 23 °C, CD₃Cl): δ 161.18 (quat. C_{Py}), 159.31 (quat. C_{Py}), 137.30 (p-C_{Py}), 135.88 (p-C_{Py}), 122.69 (m-C_{Py}), 122.45 (m-C_{Py}), 49.05 ((CH_3)₂SO), 48.35 (Py–CH₂–S), 48.24 (Py–CH₂–S). EA Found (Calculated)

$C_{16}H_{20}Cl_2N_2ORuS_3$ C 35.7 (35.34), H 3.92 (3.36), N 4.92 (4.89). ESI-HRMS (*m/z*): Found (Calcd): $C_{16}H_{20}ClN_2ORuS_3^+$: 488.9461 (488.9464). FT-IR (ATR, solid): 3214 (br), 2871 (br), 1596 (m), 1591 (m), 1459 (s), 1396 (m), 1161 (s), 1083 (s), 1012 (s), 908 (s), 855 (m), 779 (s), 718 (m), 684 (m). UV-Vis (CH₃OH), λ, nm (ε, M⁻¹ cm⁻¹): 335 (4253), 256 (7404).

Synthesis of complex 4, [Ru(N₂S₂)H(CO)(PPh₃)]Cl

In a glove box, 102.0 mg (0.372 mmol) of N₂S₂ ligand and 354.0 mg (0.372 mmol, 1 equiv.) of RuHCl(CO)(PPh₃)₃ were dissolved in a mixture containing 6 mL toluene and 3 mL of methanol. The mixture was then transferred into flame dried Schlenk flask. The flask was taken outside the glove box and heated at 80 °C for 19 hours to give a clear yellow solution. The solution was then evaporated under reduced pressure inside the glove box to yield a yellow solid, which was washed thrice with a copious amount of diethyl ether and pentane and then dried to produce **4**. Yellow crystals were grown by vapor diffusion of diethyl ether into a concentrated solution of **4** in dichloromethane. Yield: 246.4 mg (0.351 mmol - 94%). ¹H NMR (600 MHz, 23 °C, CD₂Cl₂): δ 7.58-6.88 (m, *H*PPh₃ and *H*Py, 21H), 6.46 (d, ²*J*HH = 13.5 Hz, Py–C*H₂*–S, 1H), 5.96 (d, ²*J*HH = 17.5 Hz, Py–C*H₂*–S, 1H), 5.89 (d, ²*J*HH = 17.8 Hz, Py–C*H₂*–S, 1H), 5.60 (d, ²*J*HH = 13.6 Hz, Py–C*H₂*–S, 1H), 4.32 (d, ²*J*HH = 17.1 Hz, Py–C*H₂*–S, 1H), 3.94 (d, ²*J*HH = 14.1 Hz, Py–C*H₂*–S, 1H), 3.39 (d, ²*J*HH = 17.3 Hz, 1H), 3.15 (d, ²*J*HH = 14.1 Hz, 1H), −6.68 (d, ²*J*PH = 28.9 Hz, Ru–*H*, 1H). ¹³C{¹H} NMR (151 MHz, 23 °C, CD₂Cl₂): δ 204.07 (d, ²*J*PC = 18.2 Hz, Ru–*C*O), 164.29 (quat. *C*Py), 163.32 (quat. *C*Py), 161.47 (quat. *C*Py), 160.23 (quat. *C*Py), 139.31 (d, ¹*J*PC = 25.1 Hz, quat. *C*P), 133.64 (d, ²*J*PC = 10.4 Hz, o-*C*P), 131.04 (p-*C*P), 128.88 (d, ³*J*PC = 10.4 Hz, m-*C*P), 124.51 (p-*C*Py), 124.34 (p-*C*Py), 123.77 (m-*C*Py), 123.64 (m-*C*Py), 46.18 (Py–*C*H₂–S), 44.07 (Py–*C*H₂–S), 43.73 (Py–*C*H₂–S), 42.28 (Py–*C*H₂–S). ³¹P{¹H} NMR (243 MHz, 23 °C, CD₂Cl₂): δ 62.90 (*P*Ph₃). EA Found (Calculated) $C_{33}H_{30}ClN_2OPRuS_2$: C 51.14 (50.97), H 3.91 (3.85), N 3.53 (3.50). ESI-HRMS (*m/z*): Found (Calcd): $C_{33}H_{30}N_2OPRuS_2^+$: 667.0580 (667.0575). FT-IR (ATR, solid) : 3043 (br), 2876 (br), 2173 (br), 1934 (s), 1598 (m), 1594 (m), 1480 (m), 1455 (m), 1432 (m), 1398 (m), 1311 (m), 1157 (s), 1091 (s), 998 (m), 852 (s), 788 (m), 745 (s), 724 (m), 693 (s). UV-Vis (CH₂Cl₂), λ, nm (ε, M⁻¹ cm⁻¹) : 382 (843).

Formation of 1a in acetonitrile-*d₃*.

In a glove box, 10.0 mg (0.013 mmol) of complex **1** was weighed in a 20 mL vial equipped with a stirring bar. The complex was dissolved in 1 mL of acetonitrile-*d₃*, and 1.6 mg (1.1 equiv.) of KO*t*Bu was added. The reaction mixture was stirred for 3 min and then filtered through celite to give a solution of **1a**. The solution of **1a** was directly characterized by NMR. ¹H NMR (CD₃CN, 20 °C, 400 MHz): δ 7.54 (t, ³*J*HH = 7.8 Hz, p-*H*Py, 1H), 7.29-7.25 (vt, m-*H*Py, 2H), 6.38 (dd, ³*J*HH = 8.8 Hz, 6.7 Hz, p-*H*Py, 1H), 5.94 (d, m-*H*Py, ³*J*HH = 8.8 Hz, 1H), 5.77 (d, ³*J*HH = 6.6 Hz, m-*H*Py, 1H), 4.76 (d, ²*J*HH = 18.9 Hz, Py-C*H₂*-S, 0.83H), 4.38-4.33 (m, Py-C*H₂*-S, 1.63H), 4.25 (d, ²*J*HH = 16.2 Hz, Py-C*H₂*-S, 0.77H), 4.15-4.11 (m, Py-C*H₂*-S, 1.57H), 3.57 (s, Py-C*H*-S, 0.79H). The peaks of methylene and methine groups appear underintegrated presumably due to partial exchange with CD₃CN that occurs due to local excess of base when mixing reagents, while it remains almost unchanged during the course of 16 h at RT relative to peaks of aromatic protons, suggesting that H/D exchange is

negligible once the complex is fully formed. The complex has limited stability in solution undergoing partial decomposition after the period of one day at RT. ¹³C{¹H} NMR (CD₃CN, −30 °C, 151 MHz): δ 167.87 (quat. *C*Py), 163.05 (quat. *C*Py), 162.95 (quat. *C*Py), 154.95 (quat. *C*Py), 135.87 (p-*C*Py), 130.71 (p-*C*Py), 123.75 (m-*C*Py), 120.90 (m-*C*Py), 111.18 (m-*C*Py), 101.80 (m-*C*Py), 61.70 (Py–*C*H–S), 58.48 (Py–*C*H₂–S), 49.32 (Py–*C*H₂–S), 45.53 (Py–*C*H₂–S).

NMR yield determination of 1a: In a glove box, 10.0 mg (0.013 mmol) of complex **1** was weighed in a 20-mL vial equipped with a stir bar. The complex was dissolved in 1.5 mL of acetonitrile-*d₃* and 1.6 mg (0.014 mmol, 1.1 equiv.) of KO*t*Bu were added. 1.8 μL (0.013 mmol, 1 equiv.) of mesitylene was added to the solution by microsyringe as an internal standard. The reaction mixture was stirred for 3 min. After the reaction, the solution was taken out to analyze by ¹H NMR spectroscopy. The yield of **1a** was determined by the peak of complex **1a** at 6.37 ppm against the internal standard peak at 6.80 ppm. Yield: 98%.

Protonation of 1a by HBF₄: Complex **1a** was prepared *in situ* from 10.0 mg (0.0132 mmol) of **1** with 1.6 mg (0.014 mmol) of KO*t*Bu in acetonitrile-*d₃*. After 3 minutes following treatment with a base, the orange solution of **1a** was then treated with 2.0 μL (0.015 mmol – 1.1 equiv.) of tetrafluoroboric acid diethyl ether complex (HBF₄*Et₂O). The solution color immediately changed to yellow. The formation of [(N₂S₂)Ru(MeCN)₂]²⁺ established by comparison of ¹H NMR spectrum with complex **1**.

Formation of 1b in toluene-*d₈*

In a glove box, 15.0 mg (0.020 mmol) of complex **1** was weighed in a 20 mL vial equipped with a stirrer bar. The complex was dissolved in 1.5 mL of toluene-*d₈*, and 4.5 mg (0.040 mmol, 2.0 equiv.) of KO*t*Bu were added. The reaction mixture was stirred for 3 min. The crude was filtered using an HPLC filter, leaving a brown solid in the filter, and the filtrate is collected in a second vial to give **1b**. The solution of **1b** was directly characterized by NMR spectroscopy. The orange crystals of **1b** were grown by cooling a saturated toluene solution at −20 °C. ¹H NMR (C₇D₈, −30 °C, 600 MHz): δ 6.38 (dd, ³*J*HH= 8.6, 6.6 Hz, *p*-*H*Py, 2H), 6.26 (d, ³*J*HH = 8.7 Hz, m-*H*Py, 2H), 5.76 (d, ³*J*HH = 6.5 Hz, m-*H*Py, 2H), 4.18 (s, Py–C*H*–S, 2H), 3.89 (d, ²*J*HH = 14.5 Hz, Py–C*H₂*–S, 2H), 3.73 (d, ²*J*HH = 14.5 Hz, Py–C*H₂*–S, 2H), 0.41 (s, NC–C*H₃*, 6H). ¹³C{¹H} NMR (C₇D₈, −30 °C, 151 MHz): δ 168.49 (quat. *C*Py), 156.68 (quat. *C*Py), 129.70 (p-*C*Py), 110.58 (*m*-*C*Py), 101.67 (m-*C*Py), 61.43(Py–*C*H–S), 58.23 (Py–*C*H₂–S), 1.55 (NC–*C*H₃), 1.38 (NC–*C*H₃).

NMR yield determination of 1b, general procedure: In a glovebox, the mixture of **1** and KO*t*Bu was added to toluene-*d₈*. After stirring, the reaction mixture was filtered through a syringe filter to get a clear yellow solution of **1b**. 4.0 μL (0.029 mmol) of mesitylene was added to the solution as an internal standard. The solution was taken out to analyze by ¹H NMR spectroscopy. The yield of **1b** was determined by the peak of **1b** at 4.18 ppm against the internal standard peak at 6.66 ppm. Using 0.5 equiv. to 2 equiv. of base in all cases produced similar yields of **1b**, 17-21%, limited by the solubility of **1b** in toluene. When the formed precipitate was collected and dissolved in a more polar solvent such as CD₃CN, its ¹H NMR also corresponded to **1b** showing that low solubility was the main

factor responsible for limited yield determined in non-polar solvents.

Formation of 1b in acetonitrile-d_3

In a glove box, 10.0 mg (0.013 mmol) of complex **1** was weighed in a 20 mL vial equipped with a stir bar. The complex was dissolved in 1.5 mL of acetonitrile-d_3, and 3.2 mg (0.029 mmol, 2.2 equiv.) of KO^{t}Bu was added. The reaction mixture was stirred for 3 min and then filtered through celite to give a solution of **1b**. 1.8 µL of mesitylene (0.013 mmol, 1 equiv.) was added to the solution as an internal standard. The obtained solution was characterized by ^{1}H NMR spectroscopy. The yield of **1b** was determined by the peak of **1b** at 4.18 ppm against the internal standard peak at 6.66 ppm. Yield: 80%. ^{1}H NMR (CD$_3$CN, −30 °C, 600 MHz): δ 6.28 (dd, $^3J_{HH}$ = 8.7 Hz, $^3J_{HH}$ = 6.6 Hz, p-$\textbf{\textit{H}}_{Py}$, 2H), 5.85 (d, $^3J_{HH}$ = 8.7 Hz, m-$\textbf{\textit{H}}_{Py}$, 2H), 5.53 (d, $^3J_{HH}$ = 6.5 Hz, m-$\textbf{\textit{H}}_{Py}$, 2H).

Protonation of 1b by HBF$_4$: Complex **1b** was prepared *in situ* by treatment of 10.0 mg (0.0132 mmol) of **1** with 3.7 mg (0.0331 mmol – 2.5 equiv.) of KO^{t}Bu in acetonitrile-d_3 for 3 min. To the red solution of **1b**, 4.5 µL (0.033 mmol − 2.5 equiv.) of tetrafluoroboric acid diethyl ether complex (HBF$_4$*Et$_2$O) was added with a microsyringe, and the solution color immediately changed to yellow. The formation of [(N$_2$S$_2$)Ru(MeCN)$_2$]$^{2+}$ established by comparison of ^{1}H NMR spectrum with complex **1**.

Formation of 2a in benzene-d_6

In a glove box, 10.0 mg (0.014 mmol) of **2** was added to 1 mL of benzene-d_6. To the mixture, 3.0 mg (0.025 mmol, 1.8 equiv.) of KO^{t}Bu was added to the mixture. The solution gradually became orange-red and was stirred for 20 min. After 20 minutes, the solution was filtered through a layer of celite and a clear orange solution was obtained that was characterized as **2a**. Orange crystals were grown by vapor diffusion of pentane to the benzene solution of **2a**. ^{1}H NMR (600 MHz, 23 °C, C$_6$D$_6$): δ 8.02 (t, $^3J_{HH}$ = 8.6 Hz, o-$\textbf{\textit{H}}_{PPh3}$, 6H), 7.12 (t, $^3J_{HH}$ = 6.8 Hz, p-$\textbf{\textit{H}}_{PPh3}$, 6H), 7.04 (t, $^3J_{HH}$ = 7.3 Hz, m-$\textbf{\textit{H}}_{PPh3}$, 3H), 6.33 (t, $^3J_{HH}$ = 7.6 Hz, p-$\textbf{\textit{H}}_{Py}$, 1H), 6.29 (d, $^3J_{HH}$ = 7.6 Hz, m-$\textbf{\textit{H}}_{Py}$, 1H), 6.06 (d, $^3J_{HH}$ = 7.6 Hz, m-$\textbf{\textit{H}}_{Py}$, 1H), 6.04 (dd, $^3J_{HH}$ = 9.0 Hz, p-$\textbf{\textit{H}}_{Py}$, 1H), 5.92 (d, $^3J_{HH}$ = 8.7 Hz, m-$\textbf{\textit{H}}_{Py}$, 1H), 5.06 (d, $^3J_{HH}$ = 6.6 Hz, m-$\textbf{\textit{H}}_{Py}$, 1H), 4.81 (d, $^2J_{HH}$ = 14.7 Hz, Py−C$\textbf{\textit{H}}_2$−S, 1H), 4.02 (d, $^2J_{HH}$ = 17.9 Hz, Py−C$\textbf{\textit{H}}_2$−S, 1H), 3.86 (s, Py−C$\textbf{\textit{H}}$−S, 1H), 3.82 (d, $^2J_{HH}$ = 14.8 Hz, Py−C$\textbf{\textit{H}}_2$−S, 1H), 3.23 (d, $^2J_{HH}$ = 16.5 Hz, Py−C$\textbf{\textit{H}}_2$−S, 1H), 2.96 (d, $^2J_{HH}$ = 15.9 Hz, Py−C$\textbf{\textit{H}}_2$−S, 1H), 2.76 (d, $^2J_{HH}$ = 15.9 Hz, Py−C$\textbf{\textit{H}}_2$−S, 1H). ^{13}C{^{1}H} NMR (151 MHz, 23 °C, C$_6$D$_6$): δ 167.51 (quat. $\textbf{\textit{C}}_{Py}$), 162.35 (quat. $\textbf{\textit{C}}_{Py}$), 157.94 (quat. $\textbf{\textit{C}}_{Py}$), 153.68 (quat. $\textbf{\textit{C}}_{Py}$), 136.02 (d, $^1J_{PC}$ = 40.9 Hz, quat. $\textbf{\textit{C}}_{PPh3}$), 134.57 (d, $^2J_{PC}$ = 10.1 Hz, o-$\textbf{\textit{C}}_{PPh3}$), 133.47 (o-$\textbf{\textit{C}}_{Py}$), 129.28 (m-$\textbf{\textit{C}}_{PPh3}$), 128.35 (p-$\textbf{\textit{C}}_{PPh3}$), 122.37 (m-$\textbf{\textit{C}}_{Py}$), 118.32 (m-$\textbf{\textit{C}}_{Py}$), 110.85 (m-$\textbf{\textit{C}}_{Py}$), 99.75 (m-$\textbf{\textit{C}}_{Py}$), 65.03 (Py−$\textbf{\textit{C}}$H−S), 61.20 (Py−$\textbf{\textit{C}}H_2$−S), 51.62 (Py−$\textbf{\textit{C}}H_2$−S), 48.68 (Py−$\textbf{\textit{C}}H_2$−S); (the signal of dearomatized ortho-C$_{Py}$ peak overlaps with benzene-d_6 peak and cannot be clearly detected). ^{31}P{^{1}H} NMR (243 MHz, 23 °C, C$_6$D$_6$): δ 52.37 (s, $\textbf{\textit{P}}$Ph$_3$).

A similar procedure was used to determine the yield of **2a** in benzene-d_6 in the presence of mesitylene as an internal standard. The yield of **2a** in the presence of 0.9-1.4 equiv. of KO^{t}Bu was found to be identical, 88%, after 60 min at RT. The

yield of **2a** was determined by the peak of complex **2a** at 4.81 ppm against the internal standard peak at 6.73 ppm. Using over 2 equiv. of base leads to decomposition, accelerated by an excess base. When 2 equiv. of KO^{t}Bu are used, initially formed **2a** (36% after 20 min) decomposes after 60 min, while using 3 equiv. and more leads to no detectable **2a** and the formation of a mixture of products.

Protonation of 2a by HBF$_4$: Complex **2a** was prepared iby treatment of 10.0 mg (0.0141 mmol) of **2** with 1.7 mg (0.015 mmol) of KO^{t}Bu in benzene-d_6 for 1 hour. To the orange solution of **2a**, 2.1 µL (0.016 mmol − 1.1 equiv.) of tetrafluoroboric acid diethyl ether complex (HBF$_4$*Et$_2$O) was added with a microsyringe, and the yellow precipitate was immediately formed. The benzene solvent was evaporated under vacuum to give a yellow powder, which was identified as **2(BF$_4$)** by ^{1}H NMR spectroscopy (with dichloromethane-d_2 as NMR solvent).

Similarly, protonation with 1.1 equiv of acetic acid results in the protonation of the ligand to give **2(OAc)** with identical 1H NMR spectrum corresponding to the N2S2 ligand, and an additional peak of the acetate counter anion.

Formation of 3a in benzene-d_6

In a glove box, 10.0 mg (0.019 mmol) of **3** was added to 0.7 mL of benzene-d_6. To the mixture, 2.4 mg (0.021 mmol, 1.1 equiv.) of KO^{t}Bu was added to the mixture. The mixture gradually became orange and was allowed to stir for 1 hour. After 1 hour, the solution was filtered through a layer of celite, and a clear orange solution was obtained that was characterized as **3a**. Orange crystals were grown by vapor diffusion of pentane to the benzene solution of **3a**. ^{1}H NMR (600 MHz, C$_6$D$_6$, 23 °C) δ 6.31 (t, $^3J_{HH}$ = 7.7 Hz, p-$\textbf{\textit{H}}_{Py}$, 1H), 6.21-6.20 (m, m- and p-$\textbf{\textit{H}}_{Py}$, 2H), 6.04 (d, $^3J_{HH}$ = 8.8 Hz, m-$\textbf{\textit{H}}_{Py}$, 1H), 5.89 (d, $^3J_{HH}$ = 7.7 Hz, m-$\textbf{\textit{H}}_{Py}$, 1H), 5.46 (d, $^3J_{HH}$ = 6.7 Hz, m-$\textbf{\textit{H}}_{Py}$, 1H), 4.75 (d, $^2J_{HH}$ = 15.8 Hz, Py−C$\textbf{\textit{H}}_2$−S, 1H), 4.61 (d, $^2J_{HH}$ = 14.8 Hz, Py−C$\textbf{\textit{H}}_2$−S, 1H), 3.86 (s, Py−C$\textbf{\textit{H}}$−S, 1H), 3.74 (d, $^2J_{HH}$ = 14.8 Hz, Py−C$\textbf{\textit{H}}_2$−S, 1H), 3.64 (d, $^2J_{HH}$ = 17.9 Hz, Py−C$\textbf{\textit{H}}_2$−S, 1H), 3.33 (s, (C$\textbf{\textit{H}}_3$)$_2$SO, 3H), 3.20 (d, $^2J_{HH}$ = 15.7 Hz, Py−C$\textbf{\textit{H}}_2$−S 1H), 3.08 (d, $^2J_{HH}$ = 17.9 Hz, Py−C$\textbf{\textit{H}}_2$−S, 1H), 2.50 (s, (C$\textbf{\textit{H}}_3$)$_2$SO, 3H).

NMR yield determination of 3a: In a glovebox, 5.0 mg (0.01 mmol) of **3** was combined with 2 mL of benzene-d_6; KO^{t}Bu (1.1 or 2.0 equiv) was then added. 1.3 µL (0.01 mmol, 1 equiv.) of mesitylene was added to the solution as an internal standard. The solution was placed into an NMR tube and analysed by ^{1}H NMR spectroscopy. The yield of **3a** was determined by the peak of complex **3a** at 5.46 ppm against the internal standard peak at 6.72 ppm. When 1.1 equiv. of KO^{t}Bu was used, the yield of **3a** was 29% after 20 min and further increased to 55% after 60 min. When 2.0 equiv. of KO^{t}Bu was used, no detectable **3a** was present and an intractable mixture of products formed.

Protonation of 3a by HBF$_4$: Complex **3a** was prepared *in situ* by treatment of 10.0 mg (0.0141 mmol) of **3** with 2.4 mg (0.021 mmol) of KO^{t}Bu in benzene-d_6 for 60 min. To the orange solution of **3a**, 2.9 µL (0.021 mmol − 1.1 equiv.) of tetrafluoroboric acid diethyl ether complex (HBF$_4$*Et$_2$O) was added with a microsyringe, and the yellow precipitate was immediately formed. The benzene solvent was evaporated under vacuum to give a yellow powder, which was identified as

3[BF₄] by ^1H NMR spectroscopy (with dichloromethane-d_2 as NMR solvent).

Deprotonation of complex 4

In a glove box, 14.0 mg (0.020 mmol) of **4** was added to 0.7 mL of benzene-d_6. To the mixture, 2.5 mg (0.022 mmol, 1.1 equiv.) of KO^{t}Bu was added. The mixture gradually became red and was allowed to stir for 1 hour. After 1 hour, the solution was filtered through celite and a clear red solution of **4a** was obtained that was characterized by NMR spectroscopy. ^1H NMR (600 MHz, 23 °C, C₆D₆): δ 7.82 (t, $^3J_{HH}$ = 9.6 Hz, o-**H**$_{PPh3}$, 6H), 7.06 (t, $^3J_{HH}$ = 6.9 Hz, p-**H**$_{PPh3}$, 6H), 7.02 (d, $^3J_{HH}$ = 6.9 Hz, m-**H**$_{PPh3}$, 3H), 6.67 (d, $^2J_{HH}$ = 13.7 Hz, Py–C**H**₂–S, 1H), 6.46 (d, $^2J_{HH}$ = 8.2 Hz, p-**H**$_{Py}$, 1H), 6.36 (d, $^3J_{HH}$ = 5.5 Hz, m-**H**$_{Py}$, 1H), 6.05 (vt, $^3J_{HH}$= 8.7 Hz, 6.6 Hz p-**H**$_{Py}$, 1H), 5.92 (d, $^3J_{HH}$ = 9.6 Hz, m-**H**$_{Py}$, 1H), 5.70 (d, $^2J_{HH}$ = 13.7 Hz, Py–C**H**₂–S, 1H), 4.98 (d, $^3J_{HH}$ = 6.9 Hz, m-**H**$_{Py}$, 1H), 3.90 (d, $^2J_{HH}$ = 13.7 Hz, Py–C**H**₂–S, 1H), 3.81 (s, Py–C**H**–S, 1H), 3.74 (d, $^2J_{HH}$ = 13.7 Hz, Py–C**H**₂–S, 1H), 3.46 (d, $^2J_{HH}$ = 13.7 Hz, Py–C**H**₂–S, 1H), 2.61 (d, $^2J_{HH}$ = 13.7 Hz, Py–C**H**₂–S, 1H), –6.55 (d, $^2J_{PH}$ = 28.8 Hz, Ru–**H**, 1H). $^{13}C\{^1H\}$ NMR (151 MHz, 23 °C, C₆D₆): δ 206.58 (d, $^2J_{PC}$ = 18.6 Hz, Ru–**C**O), 170.78 (quat. **C**$_{Py}$), 165.65 (quat. **C**$_{Py}$), 164.60 (quat. **C**$_{Py}$), 158.80 (quat. **C**$_{Py}$), 135.62 (m-**C**$_{Py}$), 135.24 (d, $^1J_{PC}$ = 47.7 Hz, quat. **C**$_{PPh3}$), 134.14 (d, $^2J_{PC}$ = 10.5 Hz, o-**C**$_{PPh3}$), 132.00 (p-**C**$_{Py}$), 129.77 (m-**C**$_{PPh3}$), 128.35 (p-**C**$_{PPh3}$), 123.53 (p-**C**$_{Py}$), 122.78 (m-**C**$_{Py}$), 113.50 (m-**C**$_{Py}$), 102.82 (m-**C**$_{Py}$), 59.69 (Py–**C**H–S), 58.54 (Py–**C**H₂–S), 53.32 (Py–**C**H₂–S), 43.61 (Py–**C**H₂–S), 43.25 (Py–**C**H₂–S). $^{31}P\{^1H\}$ NMR (162 MHz, 23 °C, C₆D₆): δ 67.86 (**P**Ph₃).

NMR yield determination of 4a: In a glovebox, 5.0 mg (0.007 mmol) of **4** was combined with 2 mL of benzene-d_6; KO^{t}Bu was then added (1.1, 2.0, 3.0 or 4.0 equiv.). 1.0 μL (0.01 mmol, 1 equiv.) of mesitylene was added to the solution as an internal standard. After 60 minutes, the solution was taken out for analysis by ^1H NMR spectroscopy. The yield of **4a** was determined by the peak of complex **4a** at 4.98 ppm against the internal standard peak at 6.73 ppm. The yields varied in the range of 96-99% when 1.1, 2.0, and 3.0 equiv. of KO^{t}Bu were used. In the presence of 4.0 equiv. of KO^{t}Bu, a slightly diminished yield of 77% was obtained after 60 min.

Protonation of 4a by HBF₄: Complex **4a** was prepared *in situ* by treatment of 10.0 mg (0.0142 mmol) of **1** with 1.8 mg (0.016 mmol, 1.1 equiv) of KO^{t}Bu in benzene-d_6 for 30 min. To orange solution of **4a**, 2.1 μL (0.016 mmol – 1.1 equiv) of tetrafluoroboric acid diethyl ether complex (HBF₄*Et₂O) was added with a microsyringe, and the yellow precipitate was immediately formed. The benzene solvent was evaporated under vacuum to give a yellow powder, which was identified as **4[BF₄]** by ^1H NMR spectroscopy (with dichloromethane-d_2 as NMR solvent).

Formation of complex 5.

In a glovebox, 50.0 mg (0.070 mmol) of **2** was dissolved in 15 mL of THF. To the mixture, 25.0 mg (0.223 mmol, 3.2 equiv) of potassium tert-butoxide was added. The mixture was stirred at room temperature for 1.5 hours. During this time, the solution became dark brown. The solution was then concentrated under vacuum. 2 mL of benzene was added to dissolve the solid and the obtained solution was filtered through celite and left for crystallization by vapor diffusion of pentane. The complex **5** was obtained as red crystals in very low yield, ca. 5-10 mg, as a part of the more complex mixture of unidentified products that could be isolated. ^1H NMR (600 MHz, 23 °C, THF-d_8): δ 7.50 (t, $^3J_{HH}$ = 8.6 Hz, o-**H**$_{PPh3}$, 12H), 7.16 (t, $^3J_{HH}$ = 7.2 Hz, p-**H**$_{PPh3}$, 6H), 7.10 (t, $^3J_{HH}$ = 7.6 Hz, m-**H**$_{PPh3}$, 12H), 6.34-6.29 (m, p-**H**$_{Py}$, 2H), 5.96-5.93 (m, p-**H**$_{Py}$ & m-**H**$_{Py}$, 4H), 5.73 (d, $^3J_{HH}$ = 8.3 Hz, m-**H**$_{Py}$, 2H), 5.56 (d, $^3J_{HH}$ = 6.2 Hz, m-**H**$_{Py}$, 2H), 4.95 (d, $^3J_{HH}$ = 6.2 Hz, m-**H**$_{Py}$, 2H), 3.94 (d, $^2J_{HH}$ = 14.5 Hz, Py–C**H**₂–S, 2H), 3.49 (d, $^2J_{HH}$ = 13.8 Hz, Py–C**H**₂–S, 2H), 3.47 (s, Py-C**H**(Ru)-S, 2H), 3.08 (d, $^2J_{HH}$ = 14.5 Hz, Py–C**H**₂–CH, 2H), 2.41 (d, $^2J_{HH}$ = 14.5 Hz, P–C**H**₂–CH, 2H); (proton peak of Py–C**H**(CH₂)–S overlaps with THF). $^{13}C\{^1H\}$ NMR (600 MHz, 23 °C, THF-d_8): δ 168.78 (quat. **C**$_{Py}$), 166.20 (quat. **C**$_{Py}$), 159.50 (quat. **C**$_{Py}$), 157.97 (quat. **C**$_{Py}$), 138.13 (d, $^1J_{CP}$ = 36.1 Hz, quat. **C**$_{PPh3}$), 135.31 (d, $^2J_{CP}$ = 10.1 Hz, o-C$_{PPh3}$), 130.72 (p-**C**$_{Py}$), 128.90 (p-**C**$_{PPh3}$), 128.14 (p-**C**$_{Py}$), 127.78 (d, $^3J_{CP}$ = 10.1 Hz, m-**C**$_{PPh3}$), 109.54 (m-**C**$_{Py}$), 108.81 (m-**C**$_{Py}$), 101.14 (m-**C**$_{Py}$), 100.78 (m-**C**$_{Py}$), 64.35 (Py–**C**H(CH₂)–S), 63.48 (Py–**C**H(Ru)–S), 60.30 (Py–**C**H₂–S), 59.36 (Py–**C**H₂–CH).

Computational details

All calculations were performed using density functional theory (DFT) as implemented in the Gaussian 16 suite of programs.[42] Geometry optimizations and frequency analyses were carried out without symmetry restrictions; ground states corresponded to the absence of imaginary frequencies. The initial atomic coordinates were taken from the crystal structures determined by SC-XRD. Gibbs free energies are reported as the 'Sum of electronic and thermal free energies'. The results reported in Table 2 and Figures 4 and 6 are reported for geometries optimized using M06 functional[43] and SDD (for Ru)[44]/6-311+g(d,p) (for other elements) [45-52] basis set taking into account solvent effect via SMD model.[53] This method was found to provide good match to the structural parameters from SC XRD data for complex **1b** and was previously used for computational analysis of dearomatized pincer Ru complexes.[54] Second order perturbation theory analysis data was performed using NBO 7.0.[55] CM5 (Truhlar's Charge Model 5) charges were calculated for optimized structures using Multiwfn.[56]

Conflicts of interest

There are no conflicts to declare.

Acknowledgements

Notes and references

1. C. Gunanathan and D. Milstein, *Chem. Rev.*, 2014, **114**, 12024-12087.
2. A. Mukherjee and D. Milstein, *ACS Catal.*, 2018, **8**, 11435-11469.
3. L. Alig, M. Fritz and S. Schneider, *Chem. Rev.*, 2019, **119**, 2681-2751.
4. C. Gunanathan and D. Milstein, *Acc. Chem. Res.*, 2011, **44**, 588-602.
5. J. R. Khusnutdinova and D. Milstein, *Angew. Chem. Int. Ed.*, 2015, **54**, 12236-12273.
6. H. A. Younus, W. Su, N. Ahmad, S. Chen and F. Verpoort, *Adv. Synth. Catal.*, 2015, **357**, 283-330.
7. M. Gargir, Y. Ben-David, G. Leitus, Y. Diskin-Posner, L. J. W. Shimon and D. Milstein, *Organometallics*, 2012, **31**, 6207-6214.
8. E. Fogler, E. Balaraman, Y. Ben-David, G. Leitus, L. J. W. Shimon and D. Milstein, *Organometallics*, 2011, **30**, 3826-3833.
9. T. Simler, L. Karmazin, C. Bailly, P. Braunstein and A. A. Danopoulos, *Organometallics*, 2016, **35**, 903-912.
10. T. Schaub, U. Radius, Y. Diskin-Posner, G. Leitus, L. J. W. Shimon and D. Milstein, *Organometallics*, 2008, **27**, 1892-1901.
11. E. Fogler, J. A. Garg, P. Hu, G. Leitus, L. J. W. Shimon and D. Milstein, *Chem. Eur. J.*, 2014, **20**, 15727-15731.
12. B. M. Trost and M. Rao, *Angew. Chem. Int. Ed.*, 2015, **54**, 5026-5043.
13. R. Patchett, I. Magpantay, L. Saudan, C. Schotes, A. Mezzetti and F. Santoro, *Angew. Chem. Int. Ed.*, 2013, **52**, 10352-10355.
14. D. Spasyuk, S. Smith and D. G. Gusev, *Angew. Chem. Int. Ed.*, 2012, **51**, 2772-2775.
15. Y. Morisaki, T. Ishida and Y. Chujo, *Org. Lett.*, 2006, **8**, 1029-1032.
16. A. Mondal, R. Sharma, D. Pal and D. Srimani, *Chem. Commun.*, 2021, **57**, 10363-10366.
17. D. Pal, A. Mondal and D. Srimani, *Catal. Sci. Technol.*, 2022, **12**, 3202-3208.
18. A. Mondal, R. Sharma, B. Dutta, D. Pal and D. Srimani, *J. Org. Chem.*, 2022, **87**, 3989-4000.
19. N. Biswas and D. Srimani, *J. Org. Chem.*, 2021, **86**, 10544-10554.
20. D. Spasyuk, S. Smith and D. G. Gusev, *Angew. Chem. Int. Ed.*, 2013, **52**, 2538-2542.
21. P. A. Dub, B. L. Scott and J. C. Gordon, *Organometallics*, 2015, **34**, 4464-4479.
22. P. Puylaert, R. van Heck, Y. Fan, A. Spannenberg, W. Baumann, M. Beller, J. Medlock, W. Bonrath, L. Lefort, S. Hinze and J. G. de Vries, *Chem. Eur. J.*, 2017, **23**, 8473-8481.
23. B. M. Stadler, P. Puylaert, J. Diekamp, R. van Heck, Y. Fan, A. Spannenberg, S. Hinze and J. G. de Vries, *Adv. Synth. Catal.*, 2018, **360**, 1151-1158.
24. P. Puylaert, A. Dell'Acqua, F. El Ouahabi, A. Spannenberg, T. Roisnel, L. Lefort, S. Hinze, S. Tin and J. G. de Vries, *Catal. Sci. Technol.*, 2019, **9**, 61-64.
25. M. Perez, S. Elangovan, A. Spannenberg, K. Junge and M. Beller, *ChemSusChem*, 2017, **10**, 83-86.
26. K. Das, A. Mondal and D. Srimani, *Chem. Commun.*, 2018, **54**, 10582-10585.
27. K. Das, A. Mondal, D. Pal and D. Srimani, *Org. Lett.*, 2019, **21**, 3223-3227.
28. S. P. Meneghetti, P. J. Lutz and J. Kress, *Organometallics*, 2001, **20**, 5050-5055.
29. J. R. Khusnutdinova, N. P. Rath and L. M. Mirica, *Inorg. Chem.*, 2014, **53**, 13112-13129.
30. J. Luo, N. P. Rath and L. M. Mirica, *Organometallics*, 2013, **32**, 3343-3353.
31. J. Luo, G. N. Tran, N. P. Rath and L. M. Mirica, *Inorg. Chem.*, 2020, **59**, 15659-15669.
32. S. Sinha, G. N. Tran, H. Na and L. M. Mirica, *Chem. Commun.*, 2022, **58**, 1143-1146.
33. A. Sarbajna, P. H. Patil, M. H. Dinh, O. Gladkovskaya, R. R. Fayzullin, S. Lapointe, E. Khaskin and J. R. Khusnutdinova, *Chem. Commun.*, 2019, **55**, 3282-3285.
34. T. Thomson and T. S. Stevens, *J. Chem. Soc.*, 1932, 69-73.
35. K. K. Ellis-Holder, B. P. Peppers, A. Y. Kovalevsky and S. T. Diver, *Org. Lett.*, 2006, **8**, 2511-2514.
36. J. J. Zhang and G. B. Schuster, *J. Org. Chem.*, 1988, **53**, 716-719.
37. W. Ando, *Acc. Chem. Res.*, 1977, **10**, 179-185.
38. S. Deolka, N. Tarannam, R. R. Fayzullin, S. Kozuch and E. Khaskin, *Chem. Commun.*, 2019, **55**, 11350-11353.
39. M. Vogt, O. Rivada-Wheelaghan, M. A. Iron, G. Leitus, Y. Diskin-Posner, L. J. W. Shimon, Y. Ben-David and D. Milstein, *Organometallics*, 2013, **32**, 300-308.
40. M. Feller, E. Ben-Ari, M. A. Iron, Y. Diskin-Posner, G. Leitus, L. J. W. Shimon, L. Konstantinovski and D. Milstein, *Inorganic Chemistry*, 2010, **49**, 1615-1625.
41. T. Moriguchi, S. Kitamura, K. Sakata and A. Tsuge, *Polyhedron*, 2001, **20**, 2315-2320.
42. Gaussian 16, Revision C.01, M. J. Frisch, G. W. Trucks, H. B. Schlegel, G. E. Scuseria, M. A. Robb, J. R. Cheeseman, G. Scalmani, V. Barone, G. A. Petersson, H. Nakatsuji, X. Li, M. Caricato, A. V. Marenich, J. Bloino, B. G. Janesko, R. Gomperts, B. Mennucci, H. P. Hratchian, J. V. Ortiz, A. F. Izmaylov, J. L. Sonnenberg, D. Williams-Young, F. Ding, F. Lipparini, F. Egidi, J. Goings, B. Peng, A. Petrone, T. Henderson, D. Ranasinghe, V. G. Zakrzewski, J. Gao, N. Rega, G. Zheng, W. Liang, M. Hada, M. Ehara, K. Toyota, R. Fukuda, J. Hasegawa, M. Ishida, T. Nakajima, Y. Honda, O. Kitao, H. Nakai, T. Vreven, K. Throssell, J. A. Montgomery, Jr., J. E. Peralta, F. Ogliaro, M. J. Bearpark, J. J. Heyd, E. N. Brothers, K. N. Kudin, V. N. Staroverov, T. A. Keith, R. Kobayashi, J. Normand, K. Raghavachari, A. P. Rendell, J. C. Burant, S. S. Iyengar, J. Tomasi, M. Cossi, J. M. Millam, M. Klene, C. Adamo, R. Cammi, J. W. Ochterski, R. L. Martin, K. Morokuma, O. Farkas, J. B. Foresman, and D. J. Fox, Gaussian, Inc., Wallingford CT, 2019.
43. Y. Zhao and D. G. Truhlar, *Theor. Chem. Acc.*, 2008, **120**, 215-241.
44. D. Andrae, U. Häußermann, M. Dolg, H. Stoll and H. Preuß, *Theor. Chim. Acta*, 1990, **77**, 123-141.
45. B. P. Pritchard, D. Altarawy, B. Didier, T. D. Gibsom and T. L. Windus, *J. Chem. Inf. Model.*, 2019, **59**, 4814-4820.
46. D. Feller, *J. Comput. Chem.*, 1996, **17**, 1571-1586.
47. K. L. Schuchardt, B. T. Didier, T. Elsethagen, L. Sun, V. Gurumoorthi, J. Chase, J. Li and T. L. Windus, *J. Chem. Inf. Model.*, 2007, **47**, 1045-1052.
48. T. Clark, J. Chandrasekhar, G. W. Spitznagel and P. V. R. Schleyer, *J. Comput. Chem.*, 1983, **4**, 294-301.

49.   M. M. Francl, W. J. Pietro, W. J. Hehre, J. S. Binkley, M. S. Gordon, D. J. DeFrees and J. A. Pople, *J. Chem. Phys.*, 1982, **77**, 3654-3665.

50.   R. Krishnan, J. S. Binkley, R. Seeger and J. A. Pople, *J. Chem. Phys.*, 1980, **72**, 650-654.

51.   A. D. McLean and G. S. Chandler, *J. Chem. Phys.*, 1980, **72**, 5639-5648.

52.   G. W. Spitznagel, T. Clark, P. v. R. Schleyer and W. J. Hehre, *J. Comput. Chem.*, 1987, **8**, 1109-1116.

53.   A. V. Marenich, C. J. Cramer and D. G. Truhlar, *J. Phys. Chem. B*, 2009, **113**, 6378-6396.

54.   T. P. Gonçalves and K.-W. Huang, *J. Am. Chem. Soc.*, 2017, **139**, 13442-13449.

55.   NBO 7.0. E. D. Glendening, J. K. Badenhoop, A. E. Reed, J. E. Carpenter, J. A. Bohmann, C. M. Morales, P. Karafiloglou, C. R. Landis, and F. Weinhold, Theoretical Chemistry Institute, University of Wisconsin, Madison, WI (2018).

56.   T. Lu and F. Chen, *J. Comput. Chem.*, 2012, **33**, 580-592.

Dalton Transactions Accepted Manuscript